Abstract

Understanding interactions between nanoparticles and model membranes is relevant to functional nano-composites and the fundamentals of nanotoxicity. In this study, the effect of polyamidoamine (PAMAM) dendrimers as model nanoparticles (NP) on the mesophase behaviour of 1-palmitoyl-2-oleoyl-sn-glycero-3-phosphoethanolamine (POPE) has been investigated using high-pressure small-angle X-ray scattering (HP-SAXS). The pressure-temperature ($p-T$) diagrams for POPE mesophases in excess water were obtained in the absence and presence of G2 and G4 polyamidoamine (PAMAM) dendrimers (29 Å and 45 Å in diameter, respectively) at varying NP-lipid number ratio (ν = 0.0002-0.02) over the pressure range p = 1-3000 bar and temperature range T = 20–80 °C. The $p-T$ phase diagram of POPE exhibited the L_β, L_α and H_{II} phases. Complete analysis of the phase diagrams, including the relative area pervaded by different phases, phase transition temperatures (T_t) and pressures (p_t), the lattice parameters (d-spacing), the pressure-dependence of d-spacing ($\Delta d/\Delta p$), and the structural ordering in the mesophase as gauged by the Scherrer coherence length (L) permitted insights into the size- and concentration-dependent interactions between the dendrimers and the model membrane system. The addition of dendrimers changed the phase transition pressure and temperature and resulted in the emergence of highly swollen lamellar phases, dubbed $L_{\beta\text{-den}}$ and $L_{\alpha\text{-den}}$. G4 PAMAM dendrimers at the highest concentration ν = 0.02 suppressed the formation of the H_{II} phase within the temperature range studied, whereas the addition of G2 PAMAM dendrimers at the same concentration promoted an extended mixed lamellar region in which L_α and L_β phases coexisted.

Keywords: Lipid Mesophases; PAMAM dendrimers; Nanoparticles; High-Pressure Small Angle X-ray Scattering; Nanotoxicity; Membrane Models; Cellular Uptake; Endocytosis; Synchrotron Scattering

1. Introduction

Polyamidoamine (PAMAM) dendrimers (*i.e.* dendritic polymer nanoparticles of size ~1 - 14 nm) have potential uses in a wide range of biomedical applications[1] such as gene transfection[2, 3], medical imaging[4-6], drug delivery[7-10] and as antimicrobial agents[11-13]. The mechanism of their cellular uptake[14, 15] and intracellular fate[16] has been shown to vary considerably with their generation (*i.e.* size), functionalisation, and concentration[17]. However, the exact roles of these parameters in PAMAM cellular entrance remain unclear. This is due, in part, to the variety and complexity of cellular membranes consisting of multiple species of lipids, proteins, carbohydrates and sterols[18].

Model membranes such as lipid monolayers[19-21], bilayers[22-25], multilayers and liposomes[26-28] have been developed to create simplified structural analogues[29, 30]. These models have been used to explore interactions between lipid molecules and proteins[31], pharmaceuticals[32, 33] and nanoparticles (NPs)[34] including PAMAM dendrimers[30], by observing resultant structural and energetic changes. For instance, these

membrane models have allowed for qualitative and quantitative comparisons of PAMAM dendrimer physicochemical properties on interactions with cell membranes[30].

Lipid mesophases are another example of model membranes[35, 36], with the lamellar L_α (liquid-crystalline) and L_β (gel) phases bearing structural resemblance to cell membranes[37] and the inverse hexagonal phase (H_{II}) [38, 39] considered an analogue for membrane fusion intermediate structures[40, 41]. The molecular deformations involved in membrane fusion are analogous to those found in the transitions between these phases; thus, studying the impact of dendrimers on the mesophase transitions may offer physical insight into the energetic process of nanoparticle cellular uptake *via* endocytosis mechanisms[29]. (The energetics of the mesophase transitions have also been considered in section S1 of the Supplementary Materials (SM) section.) This could pave the way for intelligent drug carrier design and inform the field of nanotoxicity, since in many cases NP cellular entry is an important route to impart toxic or medicinal effects. These mesophases are also of relevance to a number of applications. For instance, mesophases stable in excess water can facilitate the preparation of NP dispersions [42] and drug encapsulation and release[43]. Lipid mesophases have also been used as membrane protein crystallization templates[44].

The type of the mesophase formed by lipids depends upon lipid molecular architecture and concentration, as well as temperature, pH and other additives. Pressure[45] can also be used to alter the lipid molecular shape and thus its mesophase behaviour. Pressure can propagate through a sample rapidly (compared to temperature), reducing equilibrium time and with little effect on solvent properties. High pressure SAXS (HP-SAXS) has been used to study a variety of lipid mesophase systems[46-51] (see Winter *et al.*[45] for an extensive review on the effect of pressure on mesophases).

SAXS can identify liquid crystalline phases and give quantitative structural information on the mesophase structures. Ratios of the Bragg peak positions located in the plots of scattering intensity, *vs*. momentum transfer, Q, where $Q = 4\pi \sin\theta/\lambda$ (with 2θ the scattering angle and λ the X-ray wavelength) facilitate mesophase identification. For instance, the ratios of 1:2:3:4… correspond to the L_β or L_α phase, and 1:√3:2:√7… correspond to H_{II}[39, 52]. The shape of the Bragg peaks can also be analysed to obtain the coherence length and the paracrystalline disorder parameter (derived from the variation of the Bragg-peak full-width at half maximum (FWHM) with the diffraction order) to inform on the structural disorder in the mesophases.[35, 36, 53-57] The size of the mesophase domains and fluctuations in the *d*-spacing contribute to broadening of the Bragg peaks. The larger the coherence length and smaller *d*-spacing fluctuations (i.e. the smaller the paracrystalline disorder), the more ordered the mesophase[53]. Furthermore, thermal fluctuations can also have a damping effect on the intensity of high order peaks.

The lamellar *d*-spacing or the lattice repeat distance is given by

$$d = \frac{2\pi n}{Q_n} \qquad (1)$$

where Q_n is the n^{th} Bragg peak position; and the hexagonal lattice parameter *a* is given by

$$a = \frac{2}{\sqrt{3}} d \quad (2)$$

Previously Bulpett *et al.* [35] showed that the addition of 10 nm hydrophobic NPs shifted the H_{II}/L_{α} transition in the DOPE pressure-temperature ($p-T$) phase diagrams to lower temperatures, whereas 14 nm hydrophilic NPs stabilised the L_{α} region. Beddoes *et al.*[36] further studied the effect of 10 nm silica NPs on monoolein phase transitions. At high NP concentrations, the cubic gyroid (Q_{II}^{G}) phase was supressed, postulated to be due to aggregated NPs at the mesophase domain boundaries hindering the transition to the mesophases with high-curvature. However, at low concentrations, the NPs encouraged the Q_{II}^{G} phase, highlighting the complex interactions between NPs and model membranes. Aggregation of silica NPs at lamellar liquid crystal phase boundaries was also observed by Marlow *et al.* [58] resulting in an increase in stiffness and a reduction in domain size.

Recently Mendozza *et al*. [59] found that hydrophobic NPs (3-3.6 nm) were encapsulated in liquid crystalline Phytantriol bilayers, promoting an NP-concentration dependent phase transition from a cubic to a hexagonal phase. Hickel *et al.* [60] studied the influence of different antimicrobial peptides (length ~ 2.2-3.5 nm) on POPE mesophases. The H_{II} phase was supressed by all the peptides, at a concentration of 25 lipids to peptides, and a cubic (Q_{II}) or L_{α} phase was observed instead. The size of the peptide and the location of its insertion on the membrane determined which phase was favoured. Melittin (*Mel*), a predominately hydrophobic amino acid, had the greatest effect on the membrane thickness and inter-bilayer separation. This was attributed to the repulsion arising from the net positive charge of *Mel* at the membrane interface, preventing inter-membrane contact. Since the adjacent bilayers needed to approach each other closely in order to form the H_{II} phase, this may also explain the suppression of the H_{II} phase.

In this work, to understand the effect of the physicochemical properties of dendrimers on their interactions with cell membranes, two generations of PAMAM dendrimers (G2 and G4 of diameter 29 Å and 45 Å, respectively) and POPE (Figure 1; inset) in excess water have been used. The corresponding curvatures of the dendrimers are respectively J_{G2} = 7.69 $Å^{-1}$ and J_{G4} = 4.44 $Å^{-1}$, thus larger than the absolute value of the POPE spontaneous curvature. POPE has been previously found to form H_{II} phase at 74.8°C[61] and ambient pressure using differential scanning calorimetry (DSC) and SAXS . We investigated the effect of dendrimer size and concentration on the POPE H_{II}-L_{α} and L_{α}-L_{β} phase transitions by altering both temperature (in the range 20 – 80 °C) and pressure (in the range 1 – 3000 bar) using HP-SAXS, producing pressure-temperature ($p-T$) phase diagrams in the presence and absence of the dendrimers.

2. Materials and methods

2.1. Sample preparation

1-palmitoyl-2-oleoyl-sn-glycero-3-phosphoethanolamine (POPE) suspended in chloroform (25 mg/ml) was purchased from Avanti Polar Lipids (Alabama, USA) and used as received. Generation 2 (G2) and 4 (G4) polyamidoamine (PAMAM) dendrimers with primary amine surfaces, suspended in methanol (20 wt% and 10 wt% respectively) were purchased from Dendritech (Michigan, USA) and used as received. They had a nominal diameter of 29 and 45

Å respectively, with dynamic light scattering (DLS) measurements indicating diameters of 26 Å and 43 Å in methanol.

POPE, stored at -30°C, was allowed to warm to room temperature before a small quantity of the solution was transferred to a glass vial. The chloroform was then evaporated off overnight inside a vacuum oven (Heraeus Vacutherm VT 6025) at ~10 mbar and at room temperature (RT). Each sample contained approximately 25 mg of the lipid in excess water. The mesophase preparation (including those with PAMAM dendrimers) followed the procedures as described previously (Bulpett *et al.* [35] and Beddoes *et al.* [36]), and described in detail in Section S2 in SM.

2.2. High pressure SAXS (HP-SAXS) measurements

HP-SAXS measurements were performed at I22 beamline at the Diamond Light Source (Oxfordshire, UK) using a high-pressure cell.[62] An X-ray beam of size 180 x 100 μm with an energy of 18 keV (corresponding wavelength λ = 0.689 Å), and a Pilatus P3-2M detector (Dectris, Baden-Daetwill, Switzerland) was placed at a distance of 5.76 m from the sample. The detector was calibrated with silver behenate, and the collected 2D scattering patterns were integrated to produce the 1D intensity *vs. Q* plots. ~~Here, the momentum transfer $Q = 4\pi\ sin\theta/\lambda$, with 2θ the scattering angle.~~ The sample was contained in a polycarbonate capillary (2.08 ± 0.01 mm outer diameter, 0.10 ± 0.03 mm wall thickness, ~ 20 mm length) from Spectrum Plastics (Georgia, USA), which was sealed with Araldite® Instant 90 Sec G Resin (Huntsman Advanced Materials, Everberg, Belgium) cured at 60 °C for a minimum of 30 min. Once mounted in the HP-SAXS cell, the sample was subjected to pressure cycles from 1 to 4000 bar five times for further homogenisation and for checking the seal of the sample and the cell. The pressure-temperature ($p - T$) phase diagrams were constructed by varying the pressure hydrostatically from 1 to 3000 bar in 100 or 200 bar intervals, at a given temperature, which was varied from 20 to 80 °C or 25 to 75 °C in 5 or 10 °C increments at a rate of 1°C min^{-1}. The sample was allowed to equilibrate for 20 min after each temperature step and 60 s after each pressure step. After each pressure ramp, from 1 to 3000 bar, the pressure was returned to 1 bar to check for hysteresis. An exposure time of 100 ms was used throughout the experiment. After each pressure ramp, at a given temperature, the pressure was then returned to 1 bar and another SAXS image taken to check for radiation damage and hysteresis.

2.3. Data Analysis

2D diffraction patterns were reduced to 1D curves and a beamline background subtracted using software DAWN. Peaks were fitted with a Voigt function using Dawn and Igor Pro, and the peak position, the ratios of peak positions (hence the crystalline phase) and the coherence length, *L*, were determined. The *d*-spacing or lattice parameter, a, was calculated using the peak positions and Equation 1 or 2 respectively. *L* here is a measure of the size of the crystalline domains that scatter coherently and contribute to the observed diffraction peaks in the case of a lamellar phase, and is calculated from the Scherrer equation, $L = 2\pi K/\Delta Q$, where ΔQ is FWHM of the peak and *K* is a shape factor of order unity [35, 36, 53-57].

3. Results and discussion

3.1. *p-T* phase diagrams of control POPE mesophases

The *p-T* phase diagram of POPE in excess water was established as a control (Figure 1a), as it has not been previously reported. All the data points at specific pressure and temperature values where the SAXS measurements were taken are shown in Section S3; Fig. S1 in SM. In general, increasing pressure prompted structural order, whist increasing temperature encouraged disorder. At 25 °C and ambient pressure, POPE formed a mixed lamellar phase consisting of a lamellar ordered gel (L_β) and a lamellar liquid crystalline (L_α) phase (Region 2 in Figure 1a).

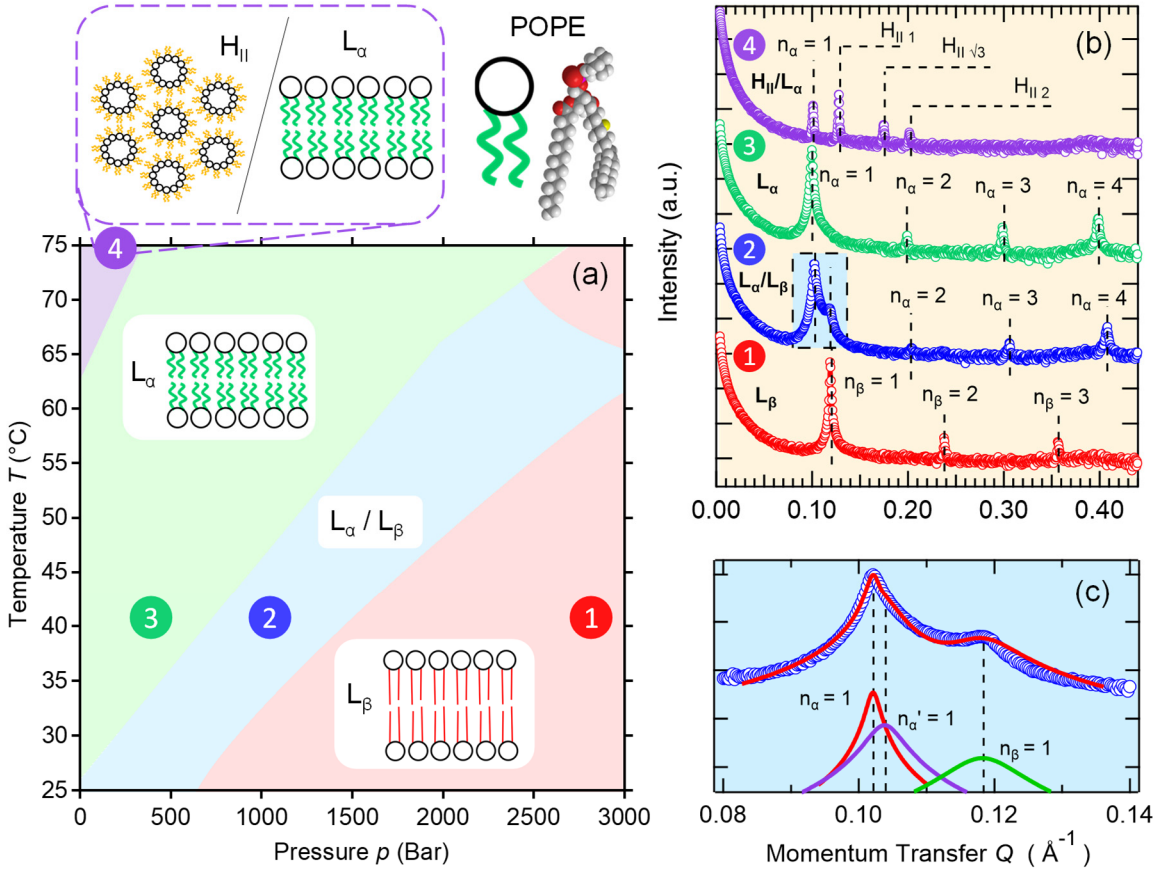

Figure 1. (a) *p-T* diagram for POPE in excess water. Four coloured mesophase regions were determined by the SAXS profiles at specific pressures and temperatures (Section S3; Fig. S1 in SM). Green: Lamellar disordered (L_α), Red: Lamellar ordered (L_β), Blue: Mixed lamellar (L_α/L_β), and Purple: Mixed lamellar disordered and hexagonal (H_{II}/L_α). (b) Representative SAXS profiles of the data points from these four phase regions, as indicated in the phase diagram. The specific curves (1), (2) and (3) were collected at T = 40 °C and p = 400, 1000 and 2800 bar, respectively. Curve (4) was collected at 75°C and 200 bar. Lamellar phases are identified by the presence of equally spaced peaks. The L_β to L_α transition is a chain-melting transition resulting in a larger lamellar *d*-spacing. (c) Enlarged view of the blue-coloured region in the SAXS profile for Point 2 (40 °C, 1000 bar) in (b), showing three individual peaks resolved by multi-peak fitting evident of a mixed lamellar phase (L_β/L_α). The peaks are fitted with a Voigt function and show

polymorphism in the L_α phase with different *d*-spacings labelled as n_α and n_α'. *d*-spacings are calculated as $d(L_\alpha)$ = 61.5 Å, $d(L_\alpha')$ = 60.5 Å and $d(L_\beta)$= 53.1 Å (error ±0.01 Å) and coherence lengths are calculated as $L(L_\alpha)$ = 3500±200 Å, $L(L_\alpha')$ = 1240 ±20 Å and $L(L_\beta)$ = 617 ± 6 Å.

This mixed phase is identified by the presence of two sets of equally spaced Bragg peaks (blue trace in Figure 1b). In some cases, only the 1st order peak for the L_β phase is present (n_β = 1 in Figure 1c) during the transition region. The peaks were fitted with a Voigt function to give the peak position and FWHM (ΔQ) which was used to calculate the coherence length *L.* The L_α phase present within the mixed lamellar phase (L_α/ L_β) showed polymorphism (Figure 2c) and so could be fitted with 3 peaks with different *d*-spacings ($d(L_\alpha)$ = 61.5 Å, $d(L_\alpha')$ = 60.5 Å and $d(L_\beta)$= 53.1 Å, error ±0.2 Å). The FWHM of these peaks was found to be $\Delta Q(n_\alpha)$ = 0.0018 $Å^{-1}$, $\Delta Q(n_\alpha')$ = 0.00504 $Å^{-1}$ and $\Delta Q(n_\beta)$ = 0.0101 $Å^{-1}$ (Error ± 0.0001 $Å^{-1}$). Using the Scherrer equation described in section 2.3 this gives coherence length values of $L(L_\alpha)$ = 3500±200 Å, $L(L_\alpha')$ = 1240 ±20 Å and $L(L_\beta)$ = 617 ± 6 Å. This shows the L_β phase had smaller coherent regions during the transition region from L_α to L_β. Further increase in the pressure to *p* = 800 bar at *T* = 25 °C caused the L_α phase to vanish and only L_β phase remained. This was indicated by a decrease in the intensity, and eventually the loss, of the L_α Bragg peaks.

At ambient pressure, increasing temperature *T* initially led to the transition to the L_α phase from the mixed L_α/ L_β phase, evident from a significant loss in the L_β peak intensity; at *T* = 65 °C, the emergence of a H_{II} phase was observed, which then coexisted with the Lα phase throughout the temperature range studied for the pure POPE sample. At higher temperatures (>70 °C), thermal fluctuations resulted in the loss of the intensity in the Bragg peaks, making phase determination difficult, and these regions are denoted as 'disordered' or 'unknown' in the *p*-*T* diagram in Section S3; Fig. S1 in the SM.

The mesophase lattice parameters (lamellar *d*-spacing, *d*, or hexagonal lattice parameter, a) are plotted as a function of pressure *p* in Figure 2. The *d*-spacing of the POPE L_α phase in excess water at 30 ° C has been reported as *d* = 52.7 ± 0.1 Å, with the ~~a~~ water channel size, d_W = 7.0 ± 0.3 Å and therefore headgroup to headgroup size d_{HH} = 45.7 ± 0.3 Å [60]. From our HP-SAXS measurements, the *d*-spacing for the L_α phase was in the range *d* = 48.8–54.5 Å and, for L_β, *d* = 59.8–63.9 Å, with the errors estimated to be ~ 0.02 Å. The *d*-spacing for the L_α and L_β phases decreased with *T* and increase with *p* as expected, consistent with more disordered structures due to increased tail fluidity at higher *T* and the opposite effect at higher *p.*

The repeat distance for the hexagonal phase varied from 61.2–64.9 Å which corresponds to a unit cell parameter of *a* = 70.6–74.9 Å (*cf*. Equation (2)). L_β to L_α is a chain-melting transition, resulting in a larger lamellar *d*-spacing of the L_α phase. The L_α phase displayed a slightly more pronounced increase in *d*-spacing with pressure than the L_β phase, with a gradient $(\Delta d/\Delta p)_T$ = 8.6 x 10^{-4} Å bar^{-1} for the L_β phase at 25°C and $(\Delta d/\Delta p)_T$ = 15 x 10^{-4} Å bar^{-1} for the L_α phase at 75°C, which can be attributed to the already highly ordered structure of the hydrophobic chains in the L_β phase. We note that the $(\Delta d/\Delta p)_T$ value for L_α agrees with that for the lipids with disordered fatty chains in the liquid crystalline phase in the literature[35, 63].

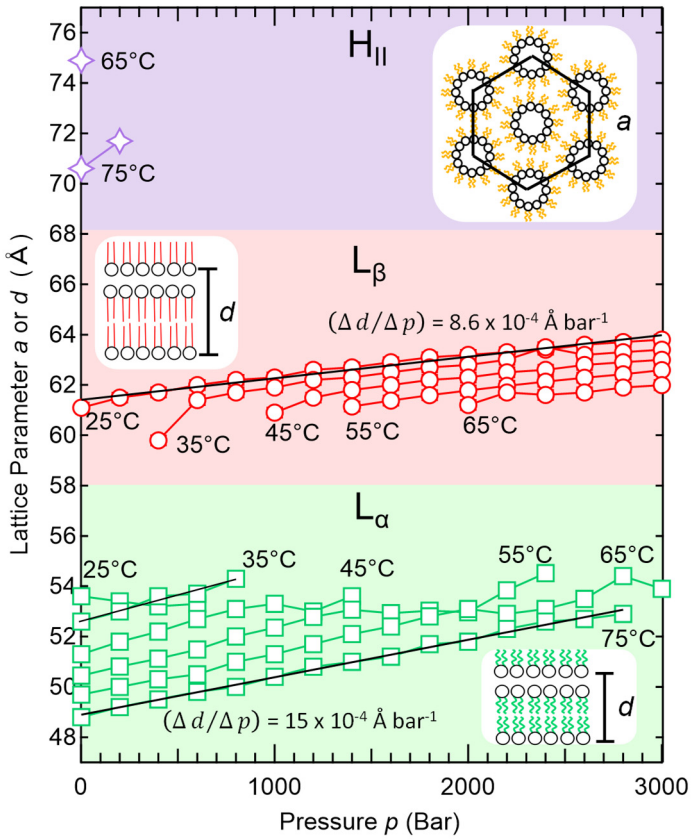

Figure 2. Lattice parameter (*d* or *a*) of the lamellar and inverted hexagonal phases of POPE as a function of pressure (errors δd and $\delta a \sim \pm 0.2$ Å and $\delta p \sim \pm 5$ bar). The L_α phase (green squares) existed between 25 and 75°C and the L_β phase (red circles) between 15 and 65 °C. The emergence of the H_{II} phase (purple diamond) occurred at 65°C and persisted to 75°C. The lines joining points are a guide for the eye. Black lines are linear fits to the *d*-*p* variations of the lamellar phases, with the gradients $\Delta d/\Delta p$ indicated.

3.2. *p*-*T* phase diagrams of POPE mesophases with G2 and G4 PAMAM dendrimers: Effects of dendrimer size and concentration

3.2.1 Mesophases in the presence of dendrimers: Emergence of new mixed lamellar phases

The *p*-*T* diagrams in Figure 3 show that the mesophase behaviour of POPE-dendrimer mixtures depended upon the dendrimer generation/size (G2 and G4) as well as the dendrimer-lipid number ratio, ν. Qualitatively, this manifested itself in the emergence of new mixed-lamellar phases and differences in the area occupied by different phase regions (*cf*. Section S4, SM).

The *p*-*T* diagram at the lowest number ratio (POPE-G2(0.0002)) with the G2 PAMAM dendrimers (Figure 3a) is similar to that of pure POPE (Figure 1b; reproduced as Figure 3d for comparison), with a smaller mixed L_α/L_β region. Increasing ν to 0.002 (POPE-G2(0.002), Figure 3b) led to the emergence of swollen lamellar structures, evident from their significantly greater *d*-spacing calculated from the positions of the Bragg peaks (*cf.* Section S5, SM), compared to that of the POPE L_α and L_β phases at ν = 0.0002. The structure of these new swollen lamellar phases was attributed to a dendrimer layer intercalated between adjacent POPE bilayers,

denoted as $L_{\alpha\text{-den}}$ and $L_{\beta\text{-den}}$, respectively. The swollen $L_{\alpha\text{-den}}$ and $L_{\beta\text{-den}}$ phases coexisted with the respective POPE lamellar phases in the mixed phase regions, denoted as $L_{\alpha\text{-den}}/L_{\alpha}$ and $L_{\beta\text{-den}}/L_{\beta}$, straddling either side of the POPE L_{α}/L_{β} mixed region, with the $L_{\alpha\text{-den}}/L_{\alpha}$ mixed phase occupying the lower p and higher T region in the phase diagram and $L_{\beta\text{-den}}/L_{\beta}$ the lower T and higher p region.

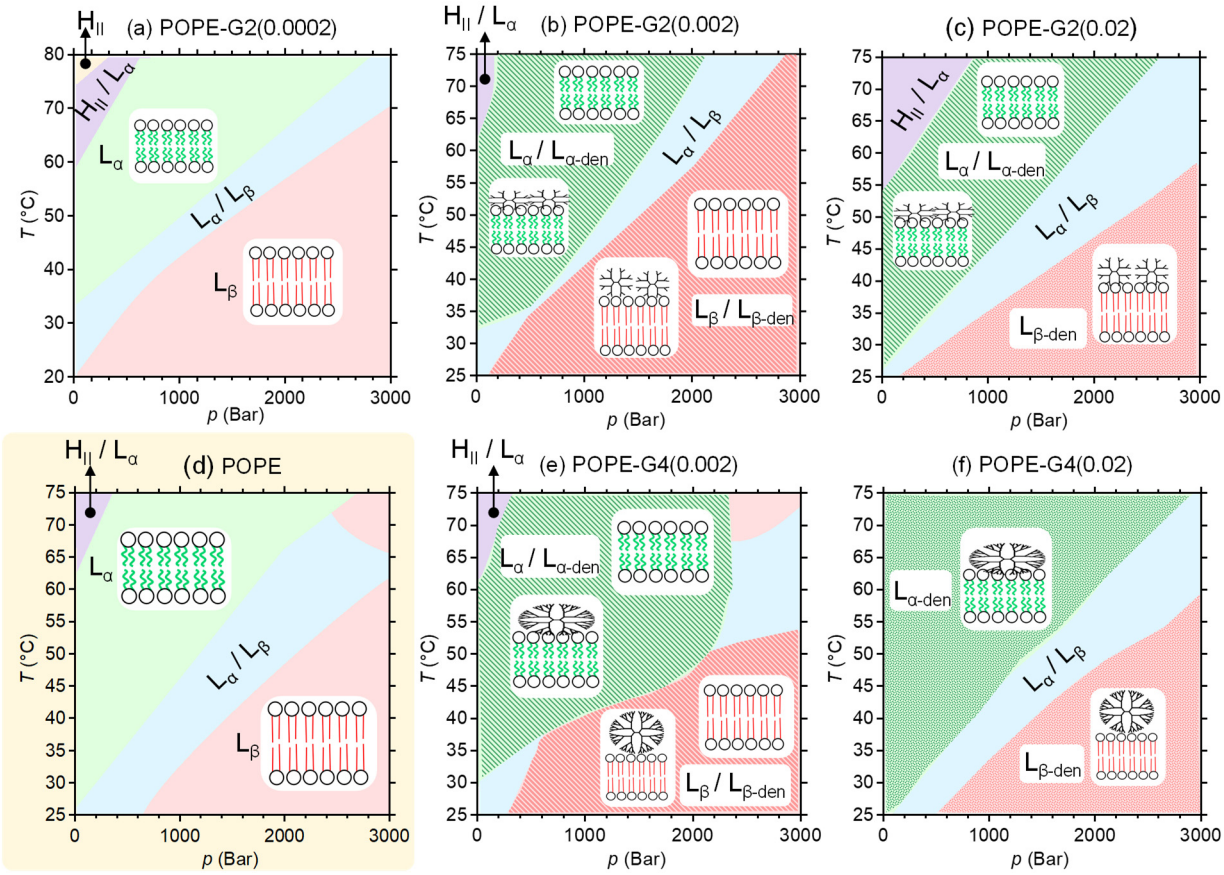

Figure 3. *p-T* phase diagrams for POPE containing G2 (a to c) and G4 (e and f) NH_2-terminated PAMAM dendrimers at dendrimer-to-lipid number ratios, $\nu = 0.02$(c and f), 0.002 (b and e) and 0.0002 (a) in excess water. The phase diagram for pure POPE (d) is reproduced from Fig. 2 and included for comparison. As the number ratio ν increased, the swollen lamellar phases ($L_{\alpha\text{-den}}$, $L_{\beta\text{-den}}$, and their mixtures $L_{\alpha}/L_{\alpha\text{-den}}$ and $L_{\beta}/L_{\beta\text{-den}}$, denoted with different fill-patterns) became more dominant. At the highest concentration of G4 PAMAM to POPE ($\nu = 0.02$), the hexagonal phase (H_{II}) was suppressed within the *p-T* range studied. Section S3; Fig. S1 in SM gives detailed phase characterisation information for each pressure-temperature point.

With further increase of ν to 0.02 (POPE-G2(0.02) and POPE-G4(0.02); Figure 3c and f, respectively), the pure POPE L_{β} phase was eradicated and replaced entirely by the swollen $L_{\beta\text{-den}}$ phase. However, the L_{α} and $L_{\alpha\text{-den}}$ phases still coexisted in a large portion of the phase diagram for the POPE-G2(0.02) sample. We note that this suppression or lack of a lamellar-to-hexagonal phase transition in POPE bilayers treated with G4 PAMAM (particularly in POPE-G4(0.02)) is consistent with a previous study which showed stable intercalation of G5 PAMAM dendrimers in cell membranes [64]. In summary, for dendrimer concentrations above $\nu = 0.0002$ (Figure 3b,c,e,f), the mixed-lamellar region is made up of a combination of all four

lamellar phases (L_α, L_β, $L_{\alpha\text{-den}}$ and $L_{\beta\text{-den}}$), and there is no new dendrimer induced phase associated with the H_{II} region.

The difference between the swelling of the $L_{\alpha\text{-den}}$ and $L_{\beta\text{-den}}$ phase (*cf*. Section S5, SM) can be attributed to the change in the interaction between dendrimers with the fluid or gel lipid phase as described in an MD simulation study by Kelly *et al* [65]. G3 PAMAM dendrimers with three different terminations (protonated primary amine ($-NH_3^+$), uncharged acetamide (-Ac), and deprotonated carboxylic acid ($-COO^-$)) were found by Kelly *et al.* to interact preferentially with lipid gel L_β phases over fluid L_α phases, forming different morphologies in contact with DMPC bilayers[65]. Dendrimers were found to deform to a greater extent against bilayers in the fluid phase and retain more of a spherical shape when interacting with the headgroups of the gel phase lipids. These simulations provide evidence that dendrimers deform to maximise contacts with both lipid headgroups and tail groups. Dendrimers contain internal hydrophobic regions that could be accessible to lipid tails upon deformation whereas the charged terminal groups would favour interaction with the lipid headgroups. Wang *et al.* also observed G3, 5, 7 and 9 NH_2-terminated PAMAM dendrimers partially intercalated into a DMPC bilayer, and flattened against the bilayer surface, forming more dendrimer-lipid contacts in MD simulations[66]. Berenyi *et al.*[67] also reported that dendrimers interacting with gel phases retained more of a ball structure and flattened out less.

It follows that there was also a new transition from the $L_{\beta\text{-den}}$ to the $L_{\alpha\text{-den}}$ phase. Given that the appearance of both the swollen $L_{\alpha\text{-den}}$ and $L_{\beta\text{-den}}$ phases coincided with their 'pure' counterparts (L_α and L_β) in the same *p*-*T* regions (*cf*. Figure 3b,e), it can be assumed that the transition from $L_{\beta\text{-den}}$ to $L_{\alpha\text{-den}}$ was also a chain-melting transition caused by the melting of the hydrophobic chains of POPE. It is thus unlikely that the dendrimers were intercalated in the hydrophobic region of the stacked bilayers, which would have disrupted the chain ordering, resulting in significant changes in the lamellar chain melting transition due to dendrimer interactions with the alkyl chain groups.

3.2.2 Effect of dendrimers on mesophase transition temperature T_t and pressure p_t

The effect of the dendrimers on the phase boundaries or transition temperature T_t/pressure p_t is most notable for POPE-G2(0.02) (Figure 3c), with a lower onset temperature of the H_{II} phase which also remained stable to higher pressures compared to POPE-G2(0.002). For instance, at 70 °C, the 1st Bragg peak associated with the spacing of the H_{II} phase was observable until p = 1400 bar. However higher order Bragg peaks (√3, 2 etc.) diminished with increasing pressure, giving an uncertainty in the phase allocation beyond p = 400 bar. This contrasts with the larger PAMAM dendrimer sample POPE-G4(0.02) (Figure 3e), where the L_α phase was stabilised and the transition to H_{II} did not occur for the temperature range studied (T_{max} = 75 °C).

Figure 4 compares the transition pressure p_t at constant temperature (T = 35 °C (a) and 65 °C (b)) and transition temperature T_t at constant pressure (p = 0 bar (c) and 2000 bar (d)) between the POPE control and the samples containing v = 0.02 and 0.002 G2 and G4 dendrimers. At T = 35 °C, the highest dendrimer number ratio v ((POPE-G2(0.02) and POPE-G4(0.02)) resulted in an increase in the transition pressure (*cf.* Figure 4a) of the mixed lamellar to $L_{\beta\text{-den}}$ transition

(G2(0.02) p_t = 1200 bar, G4(0.02) p_t = 1200 bar) compared to mixed lamellar to L_β of the POPE control (p_t = 1100 bar). The L_α to mixed lamellar transition pressure was also found to increase for all samples containing dendrimers (p_t = 600–800 bar) compared to the POPE control (p_t = 400 bar). At T = 65 °C (*cf.* Figure 4b), POPE-G2(0.002) also had a transition to the $L_\beta/L_{\beta\text{-den}}$ phase which was not observed in the control or other samples. As described above (Figure 3f), POPE-G4(0.02) had only one transition at 65 °C (*cf.* Figure 4b) from the $L_{\alpha\text{-den}}$ phase to the mixed lamellar phase at a pressure similar to the other samples (p_t = 2200 bar), due to the eradication of the H_{II}/L_α phase and stabilisation of the $L_{\alpha\text{-den}}$ phase.

At p = 0 bar (*cf.* Figure 4c), the most significant change in the transition temperature T_t was observed in the POPE-G4(0.02) sample, which showed no H_{II}/L_α or L_α/L_β phase whereas the other samples retained relatively constant T_t values for transitions from H_{II}/L_α to L_α phases and from L_α phases to the mixed L_α/L_β phase. The mixed L_α/L_β phase was also absent at p = 2000 bar (*cf.* Figure 4d) for POPE-G4(0.002), resulting in a direct phase transition from $L_{\alpha\text{-den}}$ to $L_{\beta\text{-den}}$ at T_t = 55 °C . This transition is also evident from the *p*-*T* diagrams in Figure S1 in the SM which show the individual data points. The transition from the mixed L_α/L_β phase to $L_{\beta\text{-den}}$ or the mixed $L_\beta/L_{\beta\text{-den}}$ phase was also found to occur at a higher temperature (T_t = 60 °C) for POPE-G2(0.002) and a lower temperature (T_t = 45 °C) for POPE-G2(0.02) compared to the POPE control (T_t = 50 °C).

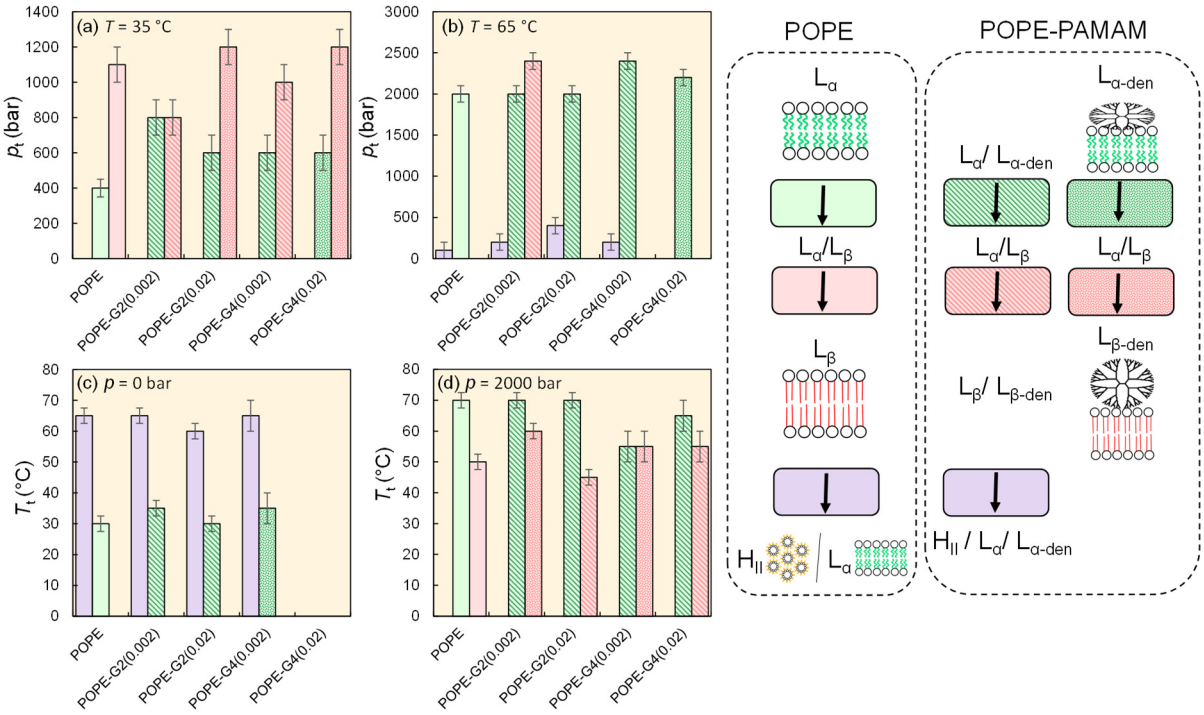

Figure 4. Phase transitions pressure p_t at (a) 35°C and (b) 65°C and phase transitions temperature T_t at (c) 0 bar and (d) 2000 bar. Errors in temperature are ± 2.5 or 5 °C and in pressure of ± 50 or 100 bar. The transitions indicated are H_{II}/L_α to L_α (lilac), L_α to L_α/L_β (green) and L_α/L_β to L_β (red). Samples with mixed L/$L_{\text{-den}}$ phases are indicated by stripes, samples with only $L_{\text{-den}}$ phases are indicated by spots. The legend on the right-hand side explains which transitions the coloured and patterned bars in the main figure represent, *e.g.* green, L_α to L_α / L_β; pink, L_α to L_β, *etc*.

The L_α to H_{II} is a low-enthalpy transition[61], and it is therefore more sensitive to perturbations than chain-melting transitions such as the L_β to L_α transition this explains why the onset of the H_{II} phase is most affected by the presence of the dendrimers. It is also interesting to note the different behaviours between G2 and G4 dendrimer samples; for POPE-G2(0.02) (Figure 4c), the coexistence of a pure L_α and dendrimer-bound, swollen $L_{\alpha\text{-den}}$ phase means that the defects, precursors to H_{II} phase formation, could still form in the 'pure' L_α POPE phase. Phase separation from the coexistence of the two phases is energetically favourable, as dendrimer clustering would reduce membrane undulations modulated by dendrimer-dendrimer charge repulsions (membrane curvature mediated attraction)[68]. The headgroup-bound dendrimers would also suppress transmembrane contact – required to form the defects and subsequent H_{II} phase. It is conceivable that this effect is dependent on the size and concentration of the dendrimers. As more dendrimers are added to the POPE mesophase, a smaller amount of a pure POPE phase remains, and the larger, headgroup-bound G4 dendrimers would create a larger physical barrier between adjacent lamellae. Although the G4 dendrimers are added at the same number ratio, they have a larger volume ratio Φ to lipid molecules than G2 dendrimers (For v = 0.02; Φ_{G2} = 13.7 and Φ_{G4} = 33.8), explaining the more pronounced effect of G4 on the phase transition boundaries compared to G2.

It has been proposed that a modification of the monolayer Gaussian curvature elastic modulus (*cf.* equations 3-5) would affect the stability of L_α phases. H_{II} formation would lead to a decrease in the energy associated with voids and defects. In the case of the POPE-dendrimer mixtures, depending upon the penetration or interaction between the dendrimers and the bilayers, either the L_α or H_{II} phase may be favoured energetically. Hickel *et al*. [60] showed that antimicrobial peptide Gramicidin S (GS, length 22 Å, positively charged) induced a cubic phase and decreased the lamellar/nonlamellar transition temperature by ~2°C, whilst another peptide Melittin (Mel; length 35 Å; positively charged) stabilized the lamellar phase, preventing the formation of an inverted hexagonal phase. Mel was presumed to 'fill the gaps' in the headgroup region, reducing the magnitude of the negative spontaneous curvature; whilst GS inserted itself into the membrane, causing membrane thinning. Dendrimers may similarly decrease the magnitude of the negative spontaneous curvature of POPE. As discussed in the introduction section, Hickel *et al.* suggested that the charge and insertion mechanism of the peptides affected the phases formed, with Mel thought to be present at the bilayer interface, resulting in repulsion between bilayers due to its net charge. The dendrimers in the intra-lamellar water channels could also be partially embedded in the membrane, resulting in repulsion between the bilayers and contributing to the large swollen bilayer *d*-spacing. Since G2 is less charged than G4, it would lead to weaker repulsion and, thus be less effective in preventing transmembrane contact. G2 is also smaller, meaning that its volume ratio to the lipid molecules is smaller than G4, leading to a smaller coverage on the membrane and a less evenly distributed coverage across intra-lamellar space. Zhang and Smith[26] postulated that a large surface coverage of dendrimers on mixed POPE/POPG vesicles prevented their close approach at high dendrimer concentrations, suppressing the extent of lipid mixing as compared to intermediate concentrations of dendrimers. Berenyi *et al.*[67] studied the effect of G5 PAMAM dendrimers on DPPC vesicles, with a complex Bragg peak observed in the obtained SAXS pattern corresponding to a highly swollen lamellar phase. The increased layer

spacing was also attributed to the dendrimers embedding in the water shells between the bilayers or the electrostatic repulsion between the dendrimer embedded in the bilayer. A larger bilayer spacing was observed at 46 °C, indicating a shape change of dendrimer when interacting with the gel or fluid phase (consistent with our observation; *cf.* Section S5, SM)

3.3.1 Effect of dendrimers on the pressure dependence of lattice spacing $(\Delta d/\Delta p)_T$

Figure 5 shows the mesophase lattice parameter as a function of pressure $(\Delta d/\Delta p)_T$ for POPE mixed with both G2 and G4 dendrimers at the highest number ratio (ν = 0.02). Compared to pure POPE (*cf.* Figure 2), it is observed that the swollen $L_{\alpha\text{-den}}$ and $L_{\beta\text{-den}}$ phases largely followed the same trend, *i.e.* a for L_α increased at a greater rate with pressure than for L_β. Linear fits, as shown in Figure 5, were used to calculate $(\Delta d/\Delta p)_T$ for the $L_{\alpha\text{-den}}$ phase at 75 °C and for the $L_{\beta\text{-den}}$ phase at 25 °C. $(\Delta d/\Delta p)_T$ was smaller for both $L_{\alpha\text{-den}}$ and $L_{\beta\text{-den}}$ phases for samples containing G2 and G4 PAMAM (ν = 0.02) compared to the 'pure' L_α and L_β POPE phases. $(\Delta d/\Delta p)_T$ values calculated from linear fits (Figure 5) are listed in Section S6; Table S1, revealing a general reduction in the rate of change of the lamellar *d*-spacing with pressure of the swollen phases with addition of PAMAM dendrimers compared to the pure phases.

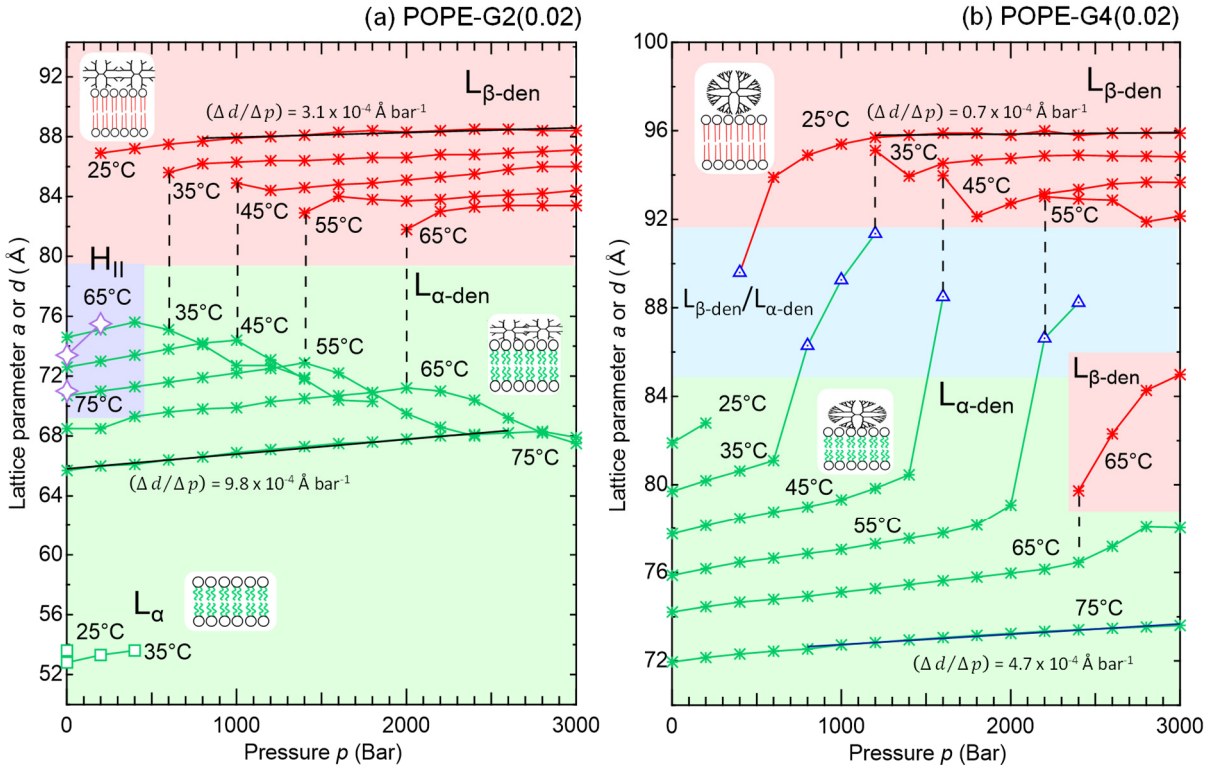

Figure 5. Comparison of the lattice parameter *a* or *d*-spacing for lamellar phases L_α (green squares), $L_{\alpha\text{-den}}$ (green stars), $L_{\beta\text{-den}}$ (red stars) and H_{II} (purple triangles) phases for (a) POPE-G2(0.02) and (b) POPE-G4(0.02) as a function of pressure. Lines between the data points are a guide for the eye. Error bars are smaller than the size of the symbols (± 0.2 Å and ± 5 bar, respectively). A transition region, where there is some ambiguity in the phase assignment, is marked with blue triangles. The black lines are the linear fits to the data for the $L_{\alpha\text{-den}}$ phase at 75 °C and $L_{\beta\text{-den}}$ phase at 25 °C. The vertical dashed lines indicate the coexisting phases at the same *p* and *T*.

Applying pressure reduces the lipid molecular volume, constraining the hydrocarbon chain motion and increasing chain ordering which leads to an increase in the *d*-spacing for the lamellar phase, as well as a decrease in the magnitude of the negative spontaneous curvature. This is opposite to the effect of temperature [69]. The *d*-spacing value of swollen lamellae incorporates the contribution from the dendrimers, and thus the $(\Delta d/\Delta p)_T$ values would also account for any pressure-induced dendrimer deformation. The reduction in the $(\Delta d/\Delta p)_{25°C}$ value for the $L_{\beta\text{-den}}$ phase compared to the L_β phase of pure POPE (~8% POPE) was most pronounced. This could indicate that the dendrimers in contact with the gel L_β phase are most resistant to deformations. Since we postulate dendrimers in contact with the L_β phase did not have significant interactions with the hydrocarbon chains of POPE, the reduction in $(\Delta d/\Delta p)_{25°C}$ would not have been due to further ordering of these chains.

As observed in Figure 5, the $(\Delta d/\Delta p)_T$ trend in the transition regions between the $L_{\alpha\text{-den}}$ and $L_{\beta\text{-den}}$ phases showed the most pronounced differences from that for the pure POPE lamellar phases (cf. Figure 3). The $L_{\alpha\text{-den}}$ lattice parameter for POPE-G2(0.02) (green stars; Figure 5a) increased initially with pressure, and then decreased upon transition to $L_{\beta\text{-den}}$ for all temperatures, resulting in a negative value of $(\Delta d/\Delta p)_T$ (for *p* = 1400 to 2400 bar, $(\Delta d/\Delta p)_{55\,°C}$ = -(52 ± 3) x 10^{-4} Å bar $^{-1}$). However, the pure POPE L_α spacing increased to a maximum before the phase transition and a negative value of $(\Delta d/\Delta p)_T$ was not observed (*cf.* Figure 2). For POPE-G4(0.02) at 35 °C (Figure 5b), the swollen $L_{\alpha\text{-den}}$ *d*-spacing increased from *d* = 81.1 Å at *p* = 600 bar to a value of *d* = 91.4 Å at *p* = 1200 bar, subsequently undergoing transition to $L_{\beta\text{-den}}$.

Due to the sudden increase in *d*-spacing with pressure, it is difficult to assign the peaks unambiguously to either $L_{\alpha\text{-den}}$ or $L_{b\text{-den}}$, and this region is therefore termed the *transition region* (blue triangle points). This extra transition region with sharply increasing *d*-spacing (in the pressure range *p* = 600 -1200 bar, $(\Delta d/\Delta p)_{35\,°C}$ = (170 ± 25) x 10^{-4} Å bar^{-1}), could be related to different interactions between dendrimers and *fluid* and *gel* phase bilayers. As the lipid bilayer approaches the L_β gel phase upon increasing pressure, the morphology of the dendrimer may change as the dendrimer is expelled from the bilayer, affecting the lattice-parameter during the transition. This corroborates with the hypothesis described above that the dendrimers are resistant to deformations against the L_β phase even with increased pressure and dendrimers are partially intercalated into the L_α phase.

The $(\Delta d/\Delta p)_{25°C}$ values of the L_β phase present in POPE-G2(0.002) and POPE-G4(0.002) samples and pure POPE were similar at 8.7 ± 0.3 x 10^{-4} Å bar $^{-1}$ and 9.7 ± 0.6 x 10^{-4} Å bar $^{-1}$ respectively (Section S6, SM), indicating that the 'pure' gel L_β phase was not significantly affected by the dendrimers. A reduction in $(\Delta d/\Delta p)_{75\,°C}$ ((9.8 ± 0.3) x 10^{-4} Å bar $^{-1}$) of $L_{\alpha\text{-den}}$ for POPE-G2(0.02) compared to L_α of pure POPE ((14.9 ± 0.3) x 10^{-4} Å bar $^{-1}$) can be ascribed to increased chain ordering due to interactions between dendrimers and lipid tails from dendrimer interdigitation into the fluid bilayer phase. The L_α and $L_{\alpha\text{-den}}$ phases coexisted in both POPE-G2(0.002) and POPE-G4(0.002); however, the Bragg peaks were damped at higher temperatures so $(\Delta d/\Delta p)_{75\,°C}$ could not be calculated for $L_{\alpha\text{-den}}$ for these two samples (*cf.* Table S1, SM). For the L_α phase in POPE-G2(0.002) and POPE-G4(0.002), $(\Delta d/\Delta p)_{75\,°C}$ = (26 ± 2) and (24 ± 1) x 10^{-4} Å bar $^{-1}$, respectively, larger than in the pure POPE system ((14.9 ± 0.3)

x 10^{-4} Å bar $^{-1}$). This again indicates that the more fluid L_α phase was affected by the intercalation of the dendrimers.

Bulpett *et al.* [35] studied the effect of 14 nm hydrophobic and 10 nm hydrophilic silica NPs on DOPE mesophases and found a smaller $(\Delta d/\Delta p)_T$ value for the pure DOPE L_α phase ($(\Delta d/\Delta p)_{35\,°C}$ ~ 13 x 10^{-4} Å bar $^{-1}$) compared to the POPE L_α phase here ($(\Delta d/\Delta p)_{35\,°C}$ = (21±2) x 10^{-4} Å bar $^{-1}$, Figure 2). They also observed a slight decrease in $(\Delta d/\Delta p)_T$ of the L_α phase upon addition of ν = 10^{-6} hydrophobic NPs ($(\Delta d/\Delta p)_{35\,°C}$ ~ 11 x 10^{-4} Å bar $^{-1}$). $(\Delta d/\Delta p)_T$ was found to increase with increasing ν for the hydrophobic NPs but remained below that of the pure DOPE L_α. No obvious trend was observed for the hydrophilic nanoparticles. However, upon addition of ν = 10^{-4} hydrophobic NPs, $(\Delta d/\Delta p)_{35\,°C}$ was found to decrease to ~ 9 x 10^{-4} Å bar $^{-1}$. From the *d*-spacing calculations, it was concluded that the NPs were not intercalated into the phases and therefore the reduction in $(\Delta d/\Delta p)_T$ was not due to particle deformations, but instead to either changes in lipid chain-packing or hydration. It was postulated that the NPs were located at phase boundaries throughout the sample to reduce the interfacial energy associated with defects in lipid packing. Although no swollen lamellar phases were observed, the reduction in $(\Delta d/\Delta p)_{35\,°C}$ is comparable to that observed in this work for the $L_{\alpha\text{-den}}$ phase of POPE-G2(0.02) compared to L_α of pure POPE.

Importantly, here the dendrimers were deformable when subject to pressure, and were intercalated into bilayers, leading to the swollen lamellar phases $L_{\alpha\text{-den}}$ and $L_{\beta\text{-den}}$. It has been suggested that nanotoxicity is influenced by the size and shape of nanoparticles[29]. Therefore, NP *deformability* (or stiffness) will also influence its toxicity and cellular entry mechanisms. For instance, softer nanogel NPs have been found to have longer circulation times in the body and lower splenic accumulation compared to stiffer nanogel NPs which would improve their therapeutic efficacy[70]. Furthermore low generation, soft dendrimer-like nanoparticles are harder to internalise due to NP deformations, and high energetic barriers that prevent membrane wrapping[71, 72]. Here, the deformability of the G2 and G4 dendrimers might have also played a role, preventing full membrane wrapping of the dendrimers in the lamellar phase.

3.3. Effect of dendrimers on the coherence length *L* of the lamellar phases

The coherence length *L* calculated by Scherrer analysis of the FWHM of the 1st order Bragg peaks (*cf*. Section 2.3) is indicative of the lower limit of the domain size along the direction of the *Q* vector. It is found to vary with different lamellar phases as well as pressure *p* and temperature *T*, which could offer insights into the structural disorder (and in turn the molecular packing) during phase transitions. Figure 6 shows the variation of *L* (*n* = 1) with *p* for the different lamellar phases (L_α, $L_{\alpha\text{-den}}$, L_β and $L_{\beta\text{-den}}$) at *T* = 45 °C. In general, the fluid lamellar phases showed more structural order than then gel lamellar phases.

L of the pure POPE L_α phase (~1000 Å; Figure 6a) was similar to that of the L_β phase during the L_α to L_β transition between 1000 and 1400 bar. Due to the complexity of the SAXS patterns observed during the transition, the coherence length was difficult to ascertain since the *n* = 1 peaks for each phase could not always be resolved due to their similar *d*-spacing and hence peak positions. A decrease in *L* for the L_α phase in the transition region may be attributed to the coexistence and thus competition for lipids between the two phases, leading to enhanced structual disorder.

L of the co-exisiting phases (L_α/$L_{\alpha\text{-den}}$ and L_β/$L_{\beta\text{-den}}$) for POPE-G2(0.002) and POPE-G4(0.002) (*cf.* Figure 6b,d) followed similar trends. The coherent domain sizes for the L_α (L ~ 3000-4000 Å) and swollen $L_{\alpha\text{-den}}$ phases (L ~ 3000-6500 Å) were the largest after the phase transition, *L* of the L_β and $L_{\beta\text{-den}}$ phases decreased and remained relatively constant with pressure. A sharp decrease in the coherence length at p = 1200 bar for POPE-G2(0.002) (Figure 6b) and p = 600 bar for POPE-G4(0.002) (Figure 6d) indicates an increase in disorder in the L_β phase. The $L_{\beta\text{-den}}$ phase was also more disordered than its $L_{\alpha\text{-den}}$ counterpart. For the samples with a larger dendrimer number ratio ν (POPE-G2(0.02) and POPE-G4(0.02); Figure 6c,e), a similar decline in the coherence length upon transition from the $L_{\alpha\text{-den}}$ to $L_{\beta\text{-den}}$ phase was also observed. This contrasts with the pure POPE sample (Figure 6a) where after an initial decline in *L* at the phase transition between 1000 and 1400 bar, *L* recovered to its initial value. This again points to the effect that the presence of the G2 and G4 dendrimers caused lamellar phase structual disorder.

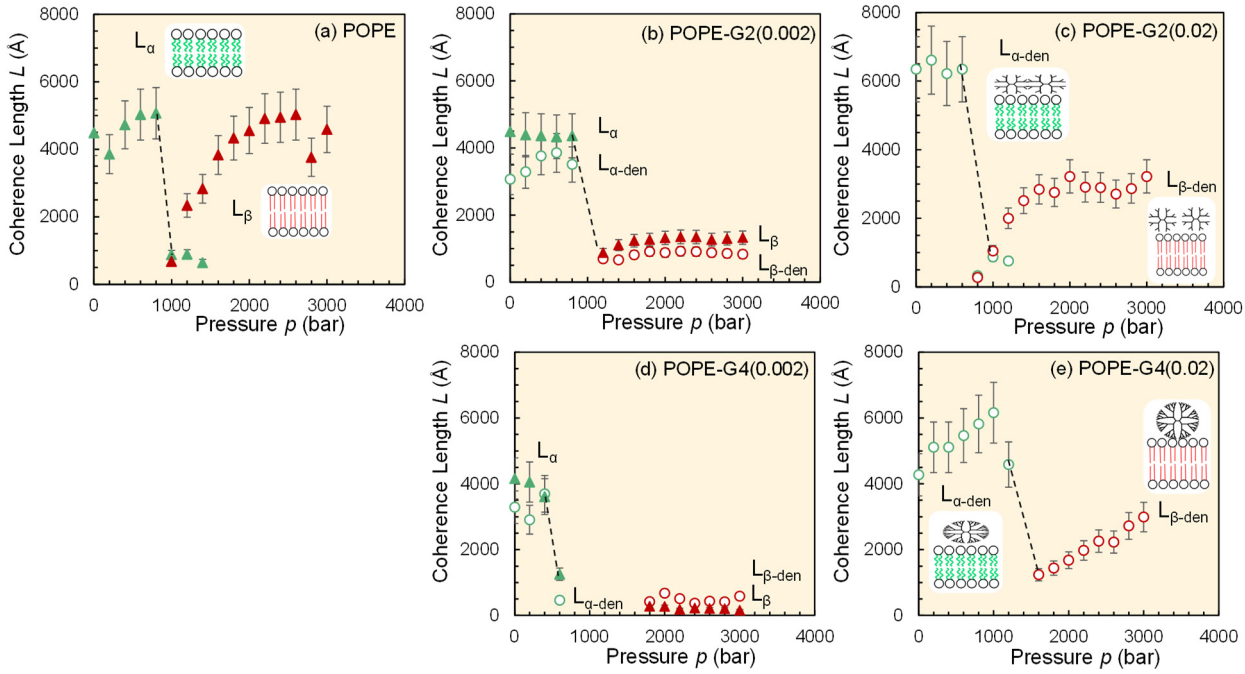

Figure 6. Coherence length *L* of lamellar phases (from Scherrer analysis of n = 1 Bragg peaks) as a function of pressure p for POPE and mixed POPE-dendrimer samples at 45°C. Error upper bound is ~15% due to the error in peak fitting for FWHM. Dotted lines indicate a phase transition.

In contrast, Calabretta *et al.* [11] found that there was no difference between the antibacterial properties of G3 and G5 dendrimers, despite the larger charge density for G5. It is conceivable that the interactions of membranes with nanoparticles depend upon the membrane composition and structural features. The complexity in biological membranes therefore continues to pose challenges to systematic physicochemical studies elucidating the mechanisms of how nanoparticles might disrupt the membrane structural integrity. It is interesting to compare the *L* values of the lamellar phases here with those of the surface anchored DOPC multilayers (stacked bilayers) reported by Sironi *et al.* that bear structural resemblance to the lamellar mesophases[53]. Dried DOPC multilayers prepared by drop-casting small unilamellar vesicles (SUVs) onto bare mica, were found to have *L* values of 1600 – 2300 Å which decreased after the multilayers were exposed to water (~1000 Å). Pure POPE

lamellar mesophases in the bulk have significantly larger L values (L_α: L ~ 3000-4000 Å) than surface anchored DOPC multilayers, thus revealing that the lamellar mesophases are more highly ordered.

4. Summary and concluding remarks

The $p - T$ diagrams for POPE mesophases in excess water have been obtained for the first time, in the presence and absence of G2 and G4 PAMAM dendrimers at lipid-NP number ratios (ν) of 0.02 and 0.002, as well as 0.0002 (in the case of G2) over the pressure range 1 - 3000 bar and temperature range 20 – 80 °C using high-pressure small angle X-ray scattering (HP-SAXS). Insights into the dendrimer size- and concentration-dependent interactions with the POPE mesophases (particularly lamellar phases) have been gained from the discussions on the effect of the dendrimers on the area pervaded by different phases in the phase diagram, phase transitions temperatures (T_t) and pressures (p_t), the lattice parameters (d-spacing), pressure-dependence of d-spacing ($\Delta d/\Delta p$), and the structural ordering in the mesophase as gauged by the Scherrer coherence length L.

The p-T diagram for POPE was established as a control, which has not been previously reported. Three phase regions were identified, gel lamellar L_β, fluid lamellar L_α, mixed lamellar L_α/L_β and mixed hexagonal and lamellar H_{II}/L_β.

Addition of G2 and G4 PAMAM dendrimers to POPE mesophases resulted in the formation of swollen lamellar phases ($L_{\alpha\text{-den}}$ and $L_{\beta\text{-den;}}$ *cf*. Figure 7a). We should acknowledge that, although the assignment of the different mesophases from the HP-SAXS profiles is unambiguous, the nanostructure of the dendrimer/lipid hybrids is complex and challenging to ascertain [30, 36]. Figure 7 presents a very simplified vision of what might have caused the observed structural changes in the mesophases. These swollen phases had different d-spacings depending upon the dendrimer size, with the large G4 dendrimers resulting in greater lamellar swelling, and they coexisted with 'pure' POPE lamellar phases at low dendrimer-lipid number ratios. Furthermore, the lamellar swelling was dependent upon the phase (gel or fluid). Less swelling occurred for fluid phase lamellae, indicating a greater change in the morphology (deformation) of dendrimers interacting with the fluid phase, consistent with the findings from MD simulations[65, 66]. The internal hydrophobic regions of the dendrimers could be accessible to lipid tails upon deformation, whereas the cationic ~~charged~~ terminal groups would favour interaction with the slightly negatively charged lipid headgroups at pH 7.0 [73] (our experimental condition). Fluid lipid tails are likely to access and thus interact more strongly with the internal hydrophobic moeities, due to increased lipid tail mobility and the reduced lipid density compared to the gel phase.

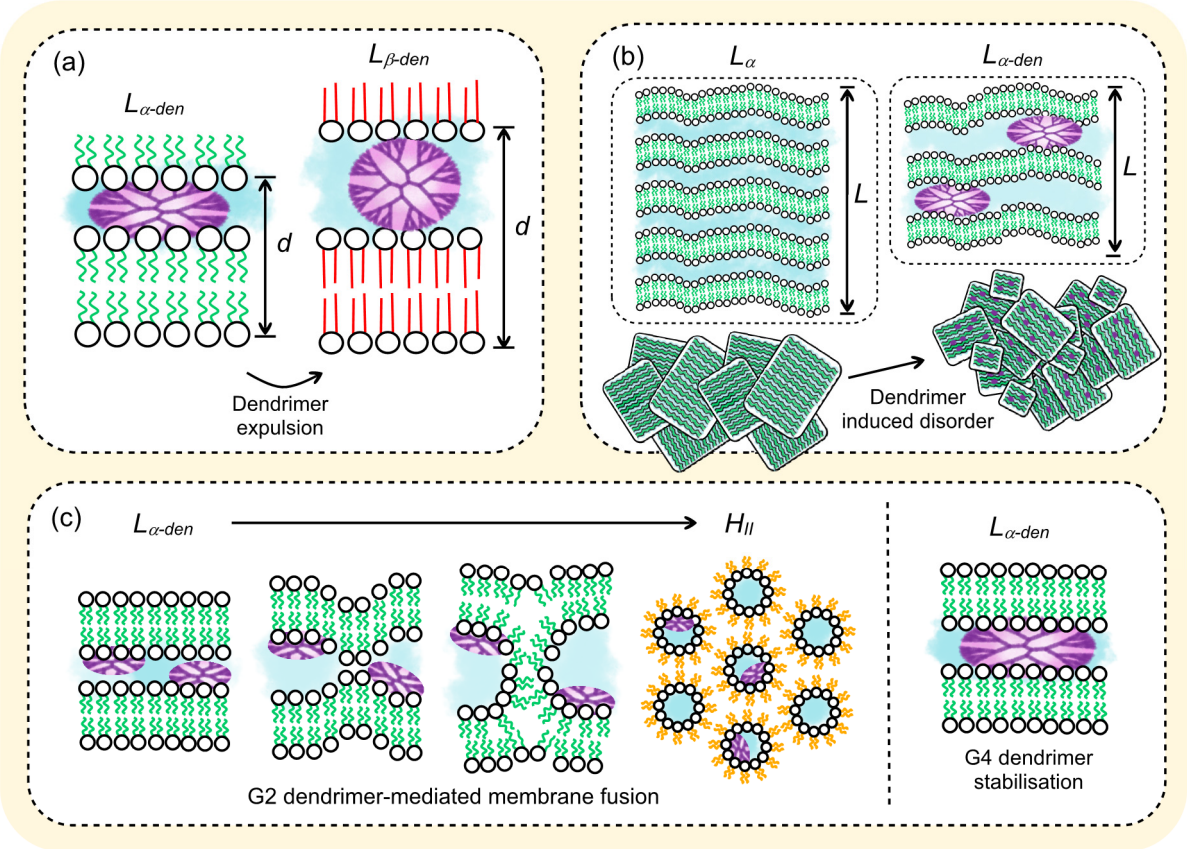

Figure 7. (a) Addition of G2 and G4 dendrimers to POPE mesophases resulted in swollen lamellar phases ($L_{\alpha\text{-den}}$ and $L_{\beta\text{-den}}$) with increased *d*-spacing. The amount of swelling was dependent on the dendrimer size and the lamellar phase (fluid or gel), with possible expulsion of the dendrimers at elevated pressures from the inter-fluid bilayers space. (b) The coherence length *L* of the fluid and gel lamellar phases decreased with the addition of G4 and G2 dendrimers, indicating increased structural disorder. (c) The phase transition from L_{α} to mixed H_{II}/L_{α} occurred at a lower temperature T_t at the highest ν of G2 dendrimers, indicating an increase in the spontaneous curvature. G4 dendrimers inhibited this transition, instead stabilising the L_{α} phase, indicating a suppression in the spontaneous curvature by prevention of inter-lamellar contact.

At the highest dendrimer-lipid number ratio ν (0.02) of G2 dendrimers, a reduction in the $L_{\alpha}/L_{\alpha\text{-den}}$ to $H_{II}/L_{\alpha\text{-den}}$ phase transition temperature T_t was observed; whereas addition of G4 at ν = 0.02 resulted in the disappearance of the $H_{II}/L_{\alpha\text{-den}}$ phase and stabilisation of the $L_{\alpha\text{-den}}$ phase (*cf*. Figure 7c). This could be rationalised by the smaller size of G2 (and hence a smaller volume ratio Φ at the same number ratio ν), which would lead to a smaller membrane coverage, allowing contact points to form between adjacent lamellae, critical for H_{II} phase formation. The greater surface coverage of G4 dendrimers may prevent inter-lamellar contact, stabilising the L_{α} phase. Furthermore, the partial insertion of the charged dendrimers into the L_{α} phase, indicated by reduced swelling compared to the L_{β} phase, could result in inter-lamellar repulsion. G4 dendrimers have 8 times as many terminal amine groups as G2, which could have resulted in greater repulsion between dendrimer-embedded lamellae. These two possible dendrimer-bilayer interactions could explain the more pronounced effect of G4 dendrimers on the phase transition boundaries.

The variation of the mesophase lattice parameter as a function of pressure $(\Delta d/\Delta p)_T$ was milder for the swollen lamellar phases ($L_{\alpha\text{-den}}$ and $L_{\beta\text{-den}}$) compared to the 'pure' POPE lamellar phases (L_α and L_β), with the swollen gel phase $L_{\beta\text{-den}}$ *d*-spacing changing the least with pressure. This finding further demonstrates the difference in dendrimer intercalation or deformation with the lamellae in the fluid or gel phases. Increasing pressure in the L_α phase could have resulted in dendrimer expulsion from the bilayers as the POPE approaches the transition to the L_β phase, resulting in a larger change of *d*-spacing with pressure (*cf*. Figure 7a). However, in the L_β phase, if the dendrimers were not intercalated, there would therefore be a smaller change in *d*-spacing with pressure. This was demonstrated by the increase in $\Delta d/\Delta p$ values in the transition region between the swollen L_α and L_β phases for POPE-G4(0.02) which could be linked to possible dendrimer expulsion from the bilayer.

Dendrimer addition was found to reduce the coherence length *L* of the POPE L_β phase, with the dendrimer swollen $L_{\beta\text{-den}}$ phase also having a significantly reduced coherence length compared to the L_α and $L_{\alpha\text{-den}}$ phases (*cf*. Figure 7b). This indicates an increase in the structural disorder in the stacked lamellae structures in the presence of the dendrimers. This effect was concentration dependent since the coexistence of the swollen and 'pure' phases resulted in a competition for the finite number of lipids between the two phases in lower number ratio systems (ν = 0.002).

Overall, these results show the importance of nanoparticle physicochemical properties (size, structure and concentration) on the interactions with model membranes, and how these interactions also depend upon the lamellar phase fluidity (L_α or L_β). These parameters are important when considering functional nanocomposite materials combining nanoparticles and organised lipid structures highlighting that the fundamental processes involved in nanoparticle cellular uptake, specifically the interactions between NPs and membranes, are of importance. We demonstrated the usefulness of HP-SAXS, a quantitative physical method employing synchrotron X-rays, in studying the complex interactions between NPs and model membranes. The knowledge gained is beneficial for the future biomedical applications of dendrimers and other NPs and is also relevant to nanocomposite materials in which nanoparticles are added to achieve enhanced properties or functionality. In future work, it will be interesting to add to the complexity of the membrane structure, e.g. by incorporating other lipids, proteins, and cholesterols, to better mimic the elastic properties of the cell membrane.

Acknowledgements

We acknowledge funding from the Engineering and Physical Science Research Council through the Bristol Centre for Functional Nanomaterials (EPSRC EP/L016648/1). We acknowledge Diamond Light Source for beamtime on I22 under proposal SM20365-1.

References

[1] N.T. Pourianazar, P. Mutlu, U. Gunduz, Bioapplications of poly(amidoamine) (PAMAM) dendrimers in nanomedicine, J Nanopart Res 16(4) (2014).
[2] P. Kesharwani, S. Banerjee, U. Gupta, M.C.I.M. Amin, S. Padhye, F.H. Sarkar, A.K. Iyer, PAMAM dendrimers as promising nanocarriers for RNAi therapeutics, Mater Today 18(10) (2015) 565-572.

[3] D.S. Conti, D. Brewer, J. Grashik, S. Avasarala, S.R.P. da Rocha, Poly(amidoamine) Dendrimer Nanocarriers and Their Aerosol Formulations for siRNA Delivery to the Lung Epithelium, Mol Pharmaceut 11(6) (2014) 1808-1822.
[4] S. Langereis, A. Dirksen, T.M. Hackeng, M.H.P. van Genderen, E.W. Meijer, Dendrimers and magnetic resonance imaging, New J Chem 31(7) (2007) 1152-1160.
[5] M. Longmire, P.L. Choyke, H. Kobayashi, Dendrimer-based contrast agents for molecular imaging, Curr Top Med Chem 8(14) (2008) 1180-6.
[6] S.L. Mekuria, T.A. Debele, H.C. Tsai, Encapsulation of Gadolinium Oxide Nanoparticle (Gd2O3) Contrasting Agents in PAMAM Dendrimer Templates for Enhanced Magnetic Resonance Imaging in Vivo, ACS Appl Mater Interfaces 9(8) (2017) 6782-6795.
[7] S. Choudhary, L. Gupta, S. Rani, K. Dave, U. Gupta, Impact of Dendrimers on Solubility of Hydrophobic Drug Molecules, Front Pharmacol 8 (2017) 261.
[8] S.S. Kulthe, Y.M. Choudhari, N.N. Inamdar, V. Mourya, Polymeric micelles: authoritative aspects for drug delivery, Des Monomers Polym 15(5) (2012) 465-521.
[9] E. Markatou, V. Gionis, G.D. Chryssikos, S. Hatziantoniou, A. Georgopoulos, C. Demetzos, Molecular interactions between dimethoxycurcumin and Pamam dendrimer carriers, Int J Pharm 339(1-2) (2007) 231-6.
[10] M. Ghaffari, G. Dehghan, F. Abedi-Gaballu, S. Kashanian, B. Baradaran, J. Ezzati Nazhad Dolatabadi, D. Losic, Surface functionalized dendrimers as controlled-release delivery nanosystems for tumor targeting, Eur J Pharm Sci 122 (2018) 311-330.
[11] M.K. Calabretta, A. Kumar, A.M. McDermott, C. Cai, Antibacterial activities of poly(amidoamine) dendrimers terminated with amino and poly(ethylene glycol) groups, Biomacromolecules 8(6) (2007) 1807-11.
[12] A.I. Lopez, R.Y. Reins, A.M. McDermott, B.W. Trautner, C. Cai, Antibacterial activity and cytotoxicity of PEGylated poly(amidoamine) dendrimers, Mol Biosyst 5(10) (2009) 1148-56.
[13] B. Wang, R.S. Navath, A.R. Menjoge, B. Balakrishnan, R. Bellair, H. Dai, R. Romero, S. Kannan, R.M. Kannan, Inhibition of bacterial growth and intramniotic infection in a guinea pig model of chorioamnionitis using PAMAM dendrimers, Int J Pharm 395(1-2) (2010) 298-308.
[14] M. Manunta, P.H. Tan, P. Sagoo, K. Kashefi, A.J. George, Gene delivery by dendrimers operates via a cholesterol dependent pathway, Nucleic Acids Res 32(9) (2004) 2730-9.
[15] M.A. Maher, H.J. Byrne, Modification of the in vitro uptake mechanism and antioxidant levels in HaCaT cells and resultant changes to toxicity and oxidative stress of G4 and G6 poly(amidoamine) dendrimer nanoparticles, Anal Bioanal Chem 408(19) (2016) 5295-307.
[16] S.P. Mukherjee, F.M. Lyng, A. Garcia, M. Davoren, H.J. Byrne, Mechanistic studies of in vitro cytotoxicity of poly(amidoamine) dendrimers in mammalian cells, Toxicol Appl Pharmacol 248(3) (2010) 259-68.
[17] L. Albertazzi, M. Serresi, A. Albanese, F. Beltram, Dendrimer internalization and intracellular trafficking in living cells, Mol Pharmaceut 7(3) (2010) 680-8.
[18] G. van Meer, A.I. de Kroon, Lipid map of the mammalian cell, J Cell Sci 124(Pt 1) (2011) 5-8.
[19] J. Cancino, T.M. Nobre, O.N. Oliveira, Jr., S.A. Machado, V. Zucolotto, A new strategy to investigate the toxicity of nanomaterials using Langmuir monolayers as membrane models, Nanotoxicology 7(1) (2013) 61-70.
[20] V. Tiriveedhi, K.M. Kitchens, K.J. Nevels, H. Ghandehari, P. Butko, Kinetic analysis of the interaction between poly(amidoamine) dendrimers and model lipid membranes, Biochim Biophys Acta 1808(1) (2011) 209-18.

[21] M. Wilde, R.J. Green, M.R. Sanders, F. Greco, Biophysical studies in polymer therapeutics: the interactions of anionic and cationic PAMAM dendrimers with lipid monolayers, J Drug Target 25(9-10) (2017) 910-918.
[22] S. Parimi, T.J. Barnes, C.A. Prestidge, PAMAM dendrimer interactions with supported lipid bilayers: a kinetic and mechanistic investigation, Langmuir 24(23) (2008) 13532-9.
[23] A. Mecke, S. Uppuluri, T.M. Sassanella, D.K. Lee, A. Ramamoorthy, J.R. Baker, Jr., B.G. Orr, M.M. Banaszak Holl, Direct observation of lipid bilayer disruption by poly(amidoamine) dendrimers, Chem Phys Lipids 132(1) (2004) 3-14.
[24] S. Hong, A.U. Bielinska, A. Mecke, B. Keszler, J.L. Beals, X. Shi, L. Balogh, B.G. Orr, J.R. Baker, Jr., M.M. Banaszak Holl, Interaction of poly(amidoamine) dendrimers with supported lipid bilayers and cells: hole formation and the relation to transport, Bioconjugate Chem 15(4) (2004) 774-82.
[25] M.L. Ainalem, R.A. Campbell, S. Khalid, R.J. Gillams, A.R. Rennie, T. Nylander, On the ability of PAMAM dendrimers and dendrimer/DNA aggregates to penetrate POPC model biomembranes, The journal of physical chemistry. B 114(21) (2010) 7229-44.
[26] Z.Y. Zhang, B.D. Smith, High-generation polycationic dendrimers are unusually effective at disrupting anionic vesicles: Membrane bending model, Bioconjugate Chem 11(6) (2000) 805-814.
[27] D. Lombardo, P. Calandra, E. Bellocco, G. Lagana, D. Barreca, S. Magazu, U. Wanderlingh, M.A. Kiselev, Effect of anionic and cationic polyamidoamine (PAMAM) dendrimers on a model lipid membrane, Biochim Biophys Acta 1858(11) (2016) 2769-2777.
[28] C.V. Kelly, M.G. Liroff, L.D. Triplett, P.R. Leroueil, D.G. Mullen, J.M. Wallace, S. Meshinchi, J.R. Baker, B.G. Orr, M.M. Banaszak Holl, Stoichiometry and Structure of Poly(amidoamine) Dendrimer-Lipid Complexes, Acs Nano 3(7) (2009) 1886-96.
[29] C.M. Beddoes, C.P. Case, W.H. Briscoe, Understanding nanoparticle cellular entry: A physicochemical perspective, Adv Colloid Interface Sci 218 (2015) 48-68.
[30] L.J. Fox, R.M. Richardson, W.H. Briscoe, PAMAM dendrimer - cell membrane interactions, Adv Colloid Interface Sci 257 (2018) 1-18.
[31] T.G. Pomorski, T. Nylander, M. Cardenas, Model cell membranes: discerning lipid and protein contributions in shaping the cell, Adv Colloid Interface Sci 205 (2014) 207-20.
[32] A.M. Seddon, D. Casey, R.V. Law, A. Gee, R.H. Templer, O. Ces, Drug interactions with lipid membranes, Chem Soc Rev 38(9) (2009) 2509-19.
[33] A.C. Alves, D. Ribeiro, C. Nunes, S. Reis, Biophysics in cancer: The relevance of drug-membrane interaction studies, Biochim Biophys Acta 1858(9) (2016) 2231-2244.
[34] L. Wu, X. Jiang, Recent developments in methodology employed to study the interactions between nanomaterials and model lipid membranes, Anal Bioanal Chem 408(11) (2016) 2743-58.
[35] J.M. Bulpett, T. Snow, B. Quignon, C.M. Beddoes, T.Y. Tang, S. Mann, O. Shebanova, C.L. Pizzey, N.J. Terrill, S.A. Davis, W.H. Briscoe, Hydrophobic nanoparticles promote lamellar to inverted hexagonal transition in phospholipid mesophases, Soft Matter 11(45) (2015) 8789-800.
[36] C.M. Beddoes, J. Berge, J.E. Bartenstein, K. Lange, A.J. Smith, R.K. Heenan, W.H. Briscoe, Hydrophilic nanoparticles stabilising mesophase curvature at low concentration but disrupting mesophase order at higher concentrations, Soft Matter 12(28) (2016) 6049-57.
[37] K. Simons, W.L. Vaz, Model systems, lipid rafts, and cell membranes, Annu Rev Biophys Biomol Struct 33(1) (2004) 269-95.

[38] T. Kaasgaard, C.J. Drummond, Ordered 2-D and 3-D nanostructured amphiphile self-assembly materials stable in excess solvent, Phys Chem Chem Phys 8(43) (2006) 4957-75.
[39] J.M. Seddon, Structure of the inverted hexagonal (HII) phase, and non-lamellar phase transitions of lipids, Biochim Biophys Acta 1031(1) (1990) 1-69.
[40] D.P. Siegel, The modified stalk mechanism of lamellar/inverted phase transitions and its implications for membrane fusion, Biophys J 76(1 Pt 1) (1999) 291-313.
[41] D.P. Siegel, R.M. Epand, The mechanism of the lamellar/inverted hexagonal phase transition and its relationship to membrane fusion: Evidence from time-resolved cryoelectron microscopy, NMR and DSC., Biophys J 72(2) (1997) Wp303-Wp303.
[42] W. Abidi, B. Pansu, R. Krishnaswamy, P. Beaunier, H. Remita, M. Impéror-Clerc, Gold nanoparticles confined in lamellar mesophases, 2011.
[43] R. Rajabalaya, M.N. Musa, N. Kifli, S.R. David, Oral and transdermal drug delivery systems: role of lipid-based lyotropic liquid crystals, Drug Des Devel Ther 11 (2017) 393-406.
[44] M. Caffrey, V. Cherezov, Crystallizing membrane proteins using lipidic mesophases, Nat Protoc 4(5) (2009) 706-31.
[45] R. Winter, C. Jeworrek, Effect of pressure on membranes, Soft Matter 5(17) (2009) 3157-3173.
[46] M. Herzog, L. Li, H.J. Galla, R. Winter, Effect of hyaluronic acid on phospholipid model membranes, Colloid Surface B 173 (2019) 327-334.
[47] J. Eisenblatter, R. Winter, Pressure effects on the structure and phase behavior of DMPC-gramicidin lipid bilayers: A synchrotron SAXS and H-2-NMR spectroscopy study, Biophys J 90(3) (2006) 956-966.
[48] C. Jeworrek, S. Uelner, R. Winter, Phase behavior and kinetics of pressure-jump induced phase transitions of bicellar lipid mixtures, Soft Matter 7(6) (2011) 2709-2719.
[49] H.M. Barriga, R.V. Law, J.M. Seddon, O. Ces, N.J. Brooks, The effect of hydrostatic pressure on model membrane domain composition and lateral compressibility, Phys Chem Chem Phys 18(1) (2016) 149-55.
[50] T.Y. Tang, N.J. Brooks, C. Jeworrek, O. Ces, N.J. Terrill, R. Winter, R.H. Templer, J.M. Seddon, Hydrostatic pressure effects on the lamellar to gyroid cubic phase transition of monolinolein at limited hydration, Langmuir 28(36) (2012) 13018-24.
[51] A. Yaghmur, M. Kriechbaum, H. Amenitsch, M. Steinhart, P. Laggner, M. Rappolt, Effects of pressure and temperature on the self-assembled fully hydrated nanostructures of monoolein-oil systems, Langmuir 26(2) (2010) 1177-85.
[52] L.J. Lis, P.J. Quinn, The Application of Synchrotron X-Radiation for the Study of Phase-Transitions in Lipid Model Membrane Systems, J Appl Crystallogr 24(1) (1991) 48-60.
[53] B. Sironi, T. Snow, C. Redeker, A. Slastanova, O. Bikondoa, T. Arnold, J. Klein, W.H. Briscoe, Structure of lipid multilayers via drop casting of aqueous liposome dispersions, Soft Matter 12(17) (2016) 3877-87.
[54] T.G. Dane, J.E. Bartenstein, B. Sironi, B.M. Mills, O. Alexander Bell, J. Emyr Macdonald, T. Arnold, C.F. Faul, W.H. Briscoe, Influence of solvent polarity on the structure of drop-cast electroactive tetra(aniline)-surfactant thin films, Phys Chem Chem Phys 18(35) (2016) 24498-505.
[55] J.M. Bulpett, A.M. Collins, N.H.M. Kaus, P.T. Cresswell, O. Bikondoa, D. Walsh, S. Mann, S.A. Davis, W.H. Briscoe, Interactions of nanoparticles with purple membrane films, J Mater Chem 22(31) (2012) 15635-15643.

[56] N.H.M. Kaus, A.M. Collins, O. Bikondoa, P.T. Cresswell, J.M. Bulpett, W.H. Briscoe, S. Mann, In situ X-ray reflectivity studies of molecular and molecular-cluster intercalation within purple membrane films, J Mater Chem C 2(27) (2014) 5447-5452.
[57] T.G. Dane, P.T. Cresswell, G.A. Pilkington, S. Lilliu, J.E. Macdonald, S.W. Prescott, O. Bikondoa, C.F.J. Faul, W.H. Briscoe, Oligo(aniline) nanofilms: from molecular architecture to microstructure, Soft Matter 9(44) (2013) 10501-10511.
[58] J.B. Marlow, M.J. Pottage, T.M. McCoy, L. De Campo, A. Sokolova, T.D.M. Bell, R.F. Tabor, Structural and rheological changes of lamellar liquid crystals as a result of compositional changes and added silica nanoparticles, Physical Chemistry Chemical Physics 20(24) (2018) 16592-16603.
[59] M. Mendozza, L. Caselli, C. Montis, S. Orazzini, E. Carretti, P. Baglioni, D. Berti, Inorganic nanoparticles modify the phase behavior and viscoelastic properties of non-lamellar lipid mesophases, Journal of colloid and interface science 541 (2019) 329-338.
[60] A. Hickel, S. Danner-Pongratz, H. Amenitsch, G. Degovics, M. Rappolt, K. Lohner, G. Pabst, Influence of antimicrobial peptides on the formation of nonlamellar lipid mesophases, Biochim Biophys Acta 1778(10) (2008) 2325-33.
[61] M. Rappolt, A. Hickel, F. Bringezu, K. Lohner, Mechanism of the lamellar/inverse hexagonal phase transition examined by high resolution x-ray diffraction, Biophys J 84(5) (2003) 3111-22.
[62] N.J. Brooks, B.L. Gauthe, N.J. Terrill, S.E. Rogers, R.H. Templer, O. Ces, J.M. Seddon, Automated high pressure cell for pressure jump x-ray diffraction, Rev Sci Instrum 81(6) (2010) 064103.
[63] M. Kato, R. Hayashi, Effects of high pressure on lipids and biomembranes for understanding high-pressure-induced biological phenomena, Biosci Biotechnol Biochem 63(8) (1999) 1321-8.
[64] S. Vaidyanathan, K.B. Anderson, R.L. Merzel, B. Jacobovitz, M.P. Kaushik, C.N. Kelly, M.A. Van Dongen, C.A. Dougherty, B.G. Orr, M.M. Banaszak Holl, Quantitative Measurement of Cationic Polymer Vector and Polymer–pDNA Polyplex Intercalation into the Cell Plasma Membrane, Acs Nano 9(6) (2015) 6097-6109.
[65] C.V. Kelly, P.R. Leroueil, B.G. Orr, M.M. Banaszak Holl, I. Andricioaei, Poly(amidoamine) dendrimers on lipid bilayers II: Effects of bilayer phase and dendrimer termination, The journal of physical chemistry. B 112(31) (2008) 9346-53.
[66] Y.L. Wang, Z.Y. Lu, A. Laaksonen, Specific binding structures of dendrimers on lipid bilayer membranes, Phys Chem Chem Phys 14(23) (2012) 8348-59.
[67] S. Berenyi, J. Mihaly, A. Wacha, O. Toke, A. Bota, A mechanistic view of lipid membrane disrupting effect of PAMAM dendrimers, Colloid Surface B 118 (2014) 164-71.
[68] T. Yue, X. Zhang, Cooperative effect in receptor-mediated endocytosis of multiple nanoparticles, Acs Nano 6(4) (2012) 3196-205.
[69] N.J. Brooks, O. Ces, R.H. Templer, J.M. Seddon, Pressure effects on lipid membrane structure and dynamics, Chem Phys Lipids 164(2) (2011) 89-98.
[70] L. Zhang, Z. Cao, Y. Li, J.-R. Ella-Menye, T. Bai, S. Jiang, Softer Zwitterionic Nanogels for Longer Circulation and Lower Splenic Accumulation, 6(8) (2012) 6681-6686.
[71] X. Yi, X. Shi, H. Gao, Cellular Uptake of Elastic Nanoparticles, Physical review letters 107(9) (2011).
[72] R. Guo, J. Mao, L.-T. Yan, Unique Dynamical Approach of Fully Wrapping Dendrimer-like Soft Nanoparticles by Lipid Bilayer Membrane, Acs Nano 7(12) (2013) 10646-10653.
[73] C. Her, Dana, Mark, Stephen, J.B, H. Steele, Thomas, The Charge Properties of Phospholipid Nanodiscs, Biophysical Journal 111(5) (2016) 989-998.